



## OPEN Bioinformatics analysis of Rho-signal transduction genes in postmenopausal osteoporosis and periodontitis

Jing Qi<sup>1,2,5</sup>, E. Liu<sup>2,5</sup>, Yunqing Pang<sup>1,3</sup>, Yu Wang<sup>4</sup> & Jing Wang<sup>1,3</sup>✉

Postmenopausal osteoporosis (PMOP) increases the risk of periodontitis (PD), yet the shared mechanisms remain unclear. Rho-signal transduction genes may play a role due to their involvement in bone remodeling. This study aimed to explore Rho-related genes as potential biomarkers linking PMOP and PD. Public transcriptomic datasets of PMOP and PD were analyzed. After PCA-based outlier removal, differentially expressed genes were identified using limma, followed by intersection analysis, KEGG enrichment, PPI network construction, and Rho pathway screening. Machine learning (Lasso, SVM-RFE) and Wilcoxon tests identified CTNNAL1 and MERTK as candidate biomarkers. GSEA, ssGSEA, and immune infiltration analyses were performed, along with construction of lncRNA/circRNA-miRNA-mRNA regulatory networks. Subcellular localization, chromosomal mapping, disease association, and molecular docking analyses were also conducted. An ovariectomy plus periodontitis (OP+PD) mouse model was used for in vivo validation. CTNNAL1 and MERTK were consistently dysregulated in both PMOP and PD datasets. They were enriched in MYC-targets-V1, allograft rejection, heme metabolism, and oxidative phosphorylation. Immune analysis revealed altered levels of CD56<sup>+</sup> bright NK cells and immature dendritic cells. Regulatory networks implicated lncRNAs such as XIST, GAS5, and NEAT1. Molecular docking indicated interactions with pinosylvin and glycitein. In vivo validation confirmed significant changes in CTNNAL1 and MERTK expression and increased bone loss and inflammation in OP+PD mice. CTNNAL1 and MERTK were identified as potential Rho-associated biomarkers showing consistent dysregulation in both PMOP and PD datasets. These biomarkers may serve as risk indicators or therapeutic candidates, warranting further validation.

**Keywords** Postmenopausal osteoporosis, Periodontitis, Bioinformatics, CTNNAL1, MERTK

Postmenopausal osteoporosis (PMOP) is a metabolic bone disease characterized by reduced bone mass and deterioration of bone microarchitecture. It is highly prevalent, affecting over 30% of women aged 50 and above<sup>1</sup>. Periodontitis (PD), the sixth most prevalent disease worldwide, is a multifactorial inflammatory condition driven by host immune responses and dysbiosis of the plaque biofilm. It leads to destruction of periodontal tissues, alveolar bone loss, and, ultimately, tooth loss<sup>2</sup>. Thus, early prevention, detection, and adequate treatment are essential to minimize the risk of complications such as fractures and tooth loss.

Clinical studies have shown that PMOP patients are more prone to developing PD. A case-control study involving 521 postmenopausal women found that osteoporosis/osteopenia significantly increased the risk of PD, particularly among nonusers of osteoporosis medication and women with more remaining teeth<sup>3</sup>. A meta-analysis of 28 observational studies with 19,611 participants revealed that PMOP is associated with worse periodontal parameters, including greater clinical attachment loss, probing depth, gingival recession, oral hygiene index, and bleeding on probing, alongside lower bone mineral density (BMD) but no significant difference in alveolar crestal height loss<sup>4</sup>. Research suggests shared mechanisms such as inflammation-driven bone remodeling, oxidative stress, and cellular senescence. Systemic low BMD is also associated with alveolar

<sup>1</sup>The First School of Clinical Medicine, Lanzhou University, 1 Donggang West Road, Chengguan District, Lanzhou, Gansu, China. <sup>2</sup>Stomatology Center of Gansu Provincial Hospital, 204 Donggang West Road, Chengguan District, Lanzhou, Gansu, China. <sup>3</sup>School of Stomatology, Lanzhou University, 1 Donggang West Road, Chengguan District, Lanzhou, Gansu, China. <sup>4</sup>Department of Endocrinology, Gansu Provincial Hospital, 204 Donggang West Road, Chengguan District, Lanzhou, Gansu, China. <sup>5</sup>Jing Qi and E. Liu contributed equally to this work. ✉email: lzukqwj@126.com

bone loss and periodontal parameters like clinical attachment loss<sup>5</sup>. However, despite these findings, effective predictive tools are lacking, and the pathological mechanisms underlying the increased susceptibility of PMOP patients to PD remain unclear.

Despite accumulating evidence that PMOP and PD share inflammation-mediated bone remodeling processes, the molecular mediators driving this interplay are not fully understood. Notably, small GTPases of the Rho family have emerged as pivotal regulators of cytoskeletal dynamics, cell adhesion, and gene transcription, all of which are essential for the maintenance of bone and periodontal tissues. Ras homologous proteins (Rho) are small GTPases prevalent in eukaryotic tissues, regulating essential cellular processes such as morphogenesis, polarity, migration, cell division, gene expression, and cytoskeletal reorganization<sup>6</sup>. Approximately 1% of human proteins are directly or indirectly influenced by Rho, implicating them in various diseases<sup>7</sup>. Functioning as molecular switches, Rho alternate between an inactive GDP-bound state and an active GTP-bound state, linking extracellular environmental changes to intracellular signaling pathways<sup>8</sup>. In bone remodeling, osteoclasts adhere to bone surfaces via  $\alpha v \beta 3$  integrins, transmitting cytoskeletal organization signals that activate molecules like c-src, syk, Vav3, and Rho GTPases. Specifically, RhoA has been shown to promote osteoclastogenesis and regulate bone remodeling through the Akt-mTOR-NFATc1 signaling pathway, contributing to osteoporosis phenotypes<sup>9,10</sup>. In PD, inflammation-induced bone resorption involves Rho. The Rho/ROCK signaling pathway plays a crucial role in actin cytoskeletal dynamics, affecting the differentiation and function of periodontal ligament cells. Modulation of this pathway influences cell behavior, including proliferation, migration, and differentiation, which are vital in periodontal tissue regeneration and homeostasis<sup>11</sup>. Despite these insights, the precise mechanisms by which Rho-signal transduction genes contributes to the pathogenesis of PMOP and PD remain to be fully elucidated.

In summary, this study employs transcriptomic analysis to identify Rho-signal transduction genes in PMOP and PD, aiming to discover potential biomarkers for both conditions. The findings are expected to enhance clinical diagnosis and treatment strategies for PMOP and PD.

## Materials and methods

### Experimental design

To explore the molecular mechanisms shared by PMOP and PD and identify potential biomarkers, we implemented a systematic bioinformatics workflow, as outlined in Fig. 1. Differential expression analysis ( $p < 0.05$  and  $|\log_2 FC| > 0.5$ ) was performed on PMOP and PD transcriptomic datasets using the limma package to identify differentially expressed genes (DEGs) for each condition. A total of 1237 DEGs (794 upregulated and 443 downregulated) were identified in the PMOP dataset, and 1244 DEGs (771 upregulated and 473 downregulated) in the PD dataset.

The intersection of DEGs from PMOP and PD datasets yielded 63 common genes. From these, 40 genes showing the same direction of change (co-upregulated or co-downregulated) in both conditions were selected. These 40 genes were cross-referenced with 2650 Rho-signal transduction genes obtained from the GeneCards database, resulting in 12 candidate genes related to the Rho pathway.

To prioritize these candidate genes, LASSO regression analysis was applied using the glmnet package with threefold cross-validation. This step yielded 8 genes: CALCRL, CCND1, CCR1, CTNNA1, FOS, MERTK, NCF1, and NRTN. Expression levels of these genes were further assessed using the Wilcoxon rank-sum test in the primary PMOP and PD datasets. Only genes showing statistically significant differential expression ( $p < 0.05$ ) and consistent trends across both the primary and validation datasets (GSE56815 for PMOP and GSE10334 for PD) were retained. As a result, CTNNA1 and MERTK were identified as robust biomarkers.

These biomarkers were subsequently subjected to additional analyses to explore their potential biological associations or involvement in disease processes, including Gene Set Enrichment Analysis (GSEA), immune infiltration analysis, transcription factor prediction, construction of molecular regulatory networks, subcellular localization, and disease association studies (Fig. 1).

### Data extraction

PMOP dataset (GSE56116), PD dataset (GSE16134), PMOP evaluation dataset (GSE56815), and PD evaluation dataset (GSE10334) were downloaded from the Gene Expression Omnibus (GEO) database. The PMOP dataset included 10 PMOP and 3 control peripheral blood samples<sup>12</sup>, and the PD dataset included 241 PD and 69 control gingival tissue samples<sup>13</sup>. The PMOP evaluation dataset consisted of 20 PMOP and 20 control peripheral blood samples<sup>14</sup>, and the PD evaluation dataset included 183 PD and 64 control gingival tissue samples<sup>15</sup>. For the PD dataset (GSE16134), raw CEL files were processed using the Robust Multi-array Average (RMA) algorithm implemented in the affy package of R. This preprocessing included background correction, quantile normalization, and probe summarization.

In addition, 2650 Rho-signal transduction genes were obtained from the GeneCards database (<http://www.genecards.org>) (Table S1–S10).

### Differentially expressed analysis

In this study, principal component analysis (PCA) was used to control quality of samples, and samples exceeding 95% confidence interval were judged as outliers and deleted in PMOP and PD datasets. DEGs between PD and control groups in PD dataset, and DEGs between PMOP and control groups in PMOP dataset were screened by differential expression analysis which was carried out by limma package (version: 3.50.1)<sup>16</sup>. Screening threshold was  $p < 0.05$  and  $|\log_2 FC| > 0.5$ . Volcano map of DEGs were generated by ggplot2 (version: 3.3.5)<sup>17</sup>.

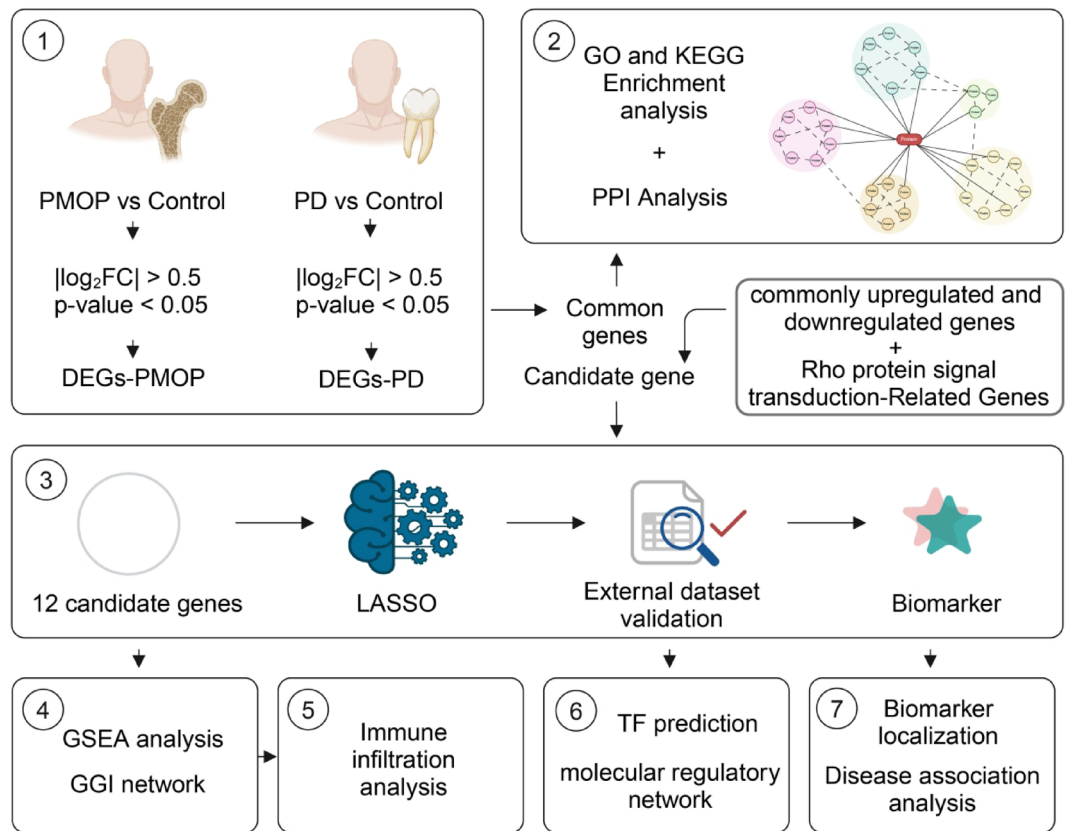


**Fig. 1.** Workflow of data analysis for identifying biomarkers related to PMOP and PD. PMOP and PD transcriptomic datasets were analyzed ( $p < 0.05$ ,  $|\log_2FC| > 0.5$ ) to identify differentially expressed genes (DEGs). Venn analysis revealed 63 common genes, which underwent KEGG enrichment and PPI network construction. Among these, commonly upregulated and downregulated genes were cross-referenced with Rho-signal transduction genes, yielding 12 candidates. LASSO narrowed them to 8 genes, which were then tested by the Wilcoxon method, identifying CTNNAL1 and MERTK as potential biomarkers. These biomarkers were validated externally and further evaluated via GSEA, immune infiltration analysis, transcription factor prediction, subcellular localization, and disease association analyses.

### Identification and analysis of candidate genes

Using the ggvnn package (version 1.7.3), DEGs identified in PMOP and PD were intersected, and the resulting common genes were then merged into a single set. KEGG enrichment analyses were carried out using the KEGG database (<https://www.kegg.jp/>)<sup>18</sup>, implemented in the clusterProfiler package (version: 4.6.0,  $p < 0.05$ )<sup>19</sup>. STRING database was utilized to explore interaction of candidate genes at protein level, and a PPI network was constructed (confidence  $> 0.4$ ). Subsequently, the commonly upregulated and commonly downregulated genes were selected from the common genes and cross-referenced with Rho-signal transduction genes using the ggvnn package, yielding the candidate genes.

### Identification of biomarkers

To identify biomarkers for PMOP and PD, we used two machine learning approaches: LASSO and SVM-RFE<sup>20</sup>. LASSO regression was performed using the glmnet R package (v4.1-2) with threefold cross-validation, yielding 8 candidate genes with non-zero coefficients. SVM-RFE was conducted with the e1071 R package on 12 initial genes. The optimal feature set was determined by the lowest error rate (0.05), resulting in 12 genes. The intersection of the two methods identified 8 overlapping genes (CALCRL, CCND1, CCR1, CTNNAL1, FOS, MERTK, NCF1, NRTN) as candidate biomarkers. Gene expression was compared between disease and control groups across discovery and validation datasets for PMOP and PD. Genes showing significant ( $p < 0.05$ ) and consistent differential expression were identified as final biomarkers.

### Corresponding analysis of biomarkers

To investigate pathways enriched by biomarkers, GSEA was conducted by clusterProfiler package. Expression of biomarkers in samples of PMOP and PD datasets was calculated by psych package (version: 2.3.9)<sup>21</sup> and sequenced. The hallmark gene set from MSigDB was reference gene set. GeneMANIA was then used to construct gene-gene interaction (GGI) network of biomarkers. Furthermore, correlation of biomarkers was explored by ggstatsplot package (version: 0.12.1)<sup>22</sup> in PD dataset.

### Immune infiltration and localization analysis

To evaluate difference between PMOP and PD with control groups, single-sample Gene Set Enrichment Analysis (ssGSEA) algorithm was conducted to calculate proportion of 28 immune cells in PMOP and PD datasets. Then difference of immune infiltration cells was compared between PMOP and PD with control groups by wilcoxon test ( $p < 0.05$ ). Spearman correlation analysis was performed to explore relationships between differential immune cells and biomarkers, and results were visualized using ggcor package (version: 0.9.8.1) to generate correlation diagrams. Moreover, subcellular and chromosome localization of biomarkers was explored by mRNALocator database and RCircos package (version: 1.2.2)<sup>23</sup>, respectively.

### Regulatory network and disease correlation analyses

To explore the regulatory mechanisms of CTNNAL1 and MERTK, we predicted upstream miRNAs using the miRDB database, identifying 14 miRNAs. LncRNAs and circRNAs targeting these miRNAs were predicted via starBase and circBank, respectively, yielding 18 lncRNAs and 34 circRNAs. These interactions were used to construct lncRNA–miRNA–mRNA and circRNA–miRNA–mRNA networks in Cytoscape (v3.9.1), totaling 73 edges (Table. S11). Transcription factors (TFs) of the biomarkers were predicted from ENCODE ChIP-seq data using NetworkAnalyst and visualized as TF–biomarker networks. TF–biomarker correlation was further analyzed using the psych package. For disease association, the CTD database was used to identify related metabolic and immune system disorders, with the top 5 visualized by ggplot2 based on inference scores.

### Animal model establishment and histological analysis

Eight-week-old female C57BL/6 mice were obtained from the Laboratory Animal Center of Lanzhou University. Mice were housed under specific pathogen-free (SPF) conditions with a 12 h light/dark cycle and ad libitum access to food and water. All animal procedures were approved by the Ethics Committee of Gansu Provincial Hospital (approval number: 2022-13). Mice were randomly divided into two groups: Sham and ovariectomy plus periodontitis (OP+PD). Osteoporosis was induced by bilateral ovariectomy under 0.3% pentobarbital sodium anesthesia (0.5 mL/100 g, i.p.). Four weeks after surgery, periodontitis was induced by ligation of the maxillary second molar with 6-0 silk suture and local application of Porphyromonas gingivalis suspension ( $1 \times 10^7$  CFU/mL) every other day for three times. Mice were euthanized at 8 weeks, and maxillary bone and femurs were harvested. Tissues were fixed in 4% paraformaldehyde for 24 h and decalcified in 19% EDTA. Paraffin sections were stained with hematoxylin and eosin (H&E) to assess trabecular bone structure and inflammatory infiltration. Alveolar bone resorption was evaluated by methylene blue staining of maxillae after soft tissue removal.

### Quantitative RT–PCR

Total RNA was extracted from gingival tissues using TRIzol reagent (Invitrogen, USA) following the manufacturer's instructions. cDNA synthesis was performed using the PrimeScript™ RT Master Mix Kit (TaKaRa, Dalian, China). Quantitative PCR was conducted using SYBR Green Master Mix (ABclonal Technology, China) on a CFX96 Real-Time PCR Detection System (Bio-Rad, USA). The relative mRNA levels of CTNNAL1 and MERTK were normalized to  $\beta$ -actin using the  $2^{-\Delta\Delta C_t}$  method. Primer sequences are listed in Table S12.

### Western blotting

Total protein was extracted from gingival tissues using RIPA lysis buffer supplemented with protease and phosphatase inhibitors (Beyotime, China). Protein concentrations were quantified using the BCA Protein Assay Kit (Thermo Fisher Scientific, USA). Equal amounts of protein (20–30  $\mu$ g) were separated on 10% SDS-PAGE gels and transferred onto PVDF membranes (Millipore, USA). Membranes were blocked in 5% BSA for 1 h at room temperature and incubated overnight at 4 °C with primary antibodies against CTNNAL1 (Abcam, ab96184, 1:1000), MERTK (Proteintech, 27900-1-AP, 1:1000), and  $\beta$ -actin (Proteintech, 66009-1-Ig, 1:3000). After washing, membranes were incubated with HRP-conjugated secondary antibodies (1:5000) for 1 h. Protein bands were visualized using enhanced chemiluminescence (ECL) substrate (Millipore), and band intensity was quantified using ImageJ software.

### ELISA for inflammatory cytokines

Blood samples were collected from the retro-orbital sinus. Serum was separated by centrifugation and stored at  $-80$  °C. The levels of TNF- $\alpha$ , IL-1 $\beta$ , IL-6, and IL-4 were measured using commercial ELISA kits (Multi Sciences, China) according to the manufacturer's protocols. Absorbance was measured at 450 nm using a microplate reader.

### Statistical analysis

R software (version: 4.2.3) was used to process and analyze data. Statistical significance between two groups was performed via Wilcoxon rank-sum test. The  $p < 0.05$  was considered statistically significant.

## Results

### Differential expression of PD and PMOP datasets

Differential expression analysis was performed on the PMOP and PD datasets. To ensure the quality of the samples, PCA was conducted to detect and exclude outliers, defined as samples beyond the 95% confidence interval. In PMOP dataset, no outliers were identified (Fig. 2A). However, in PD dataset, 31 samples were excluded as outliers, leaving a final sample distribution of PD : Control = 214:65 (Fig. 2B). Subsequently, differential gene expression analysis was carried out using the R package limma to compare gene expression levels between experimental and control groups. Applying thresholds of  $|\log_2 FC| > 0.5$  and  $p$  value  $< 0.05$ , a total of 1237 DEGs were identified for PMOP vs. Control, including 794 upregulated and 443 downregulated

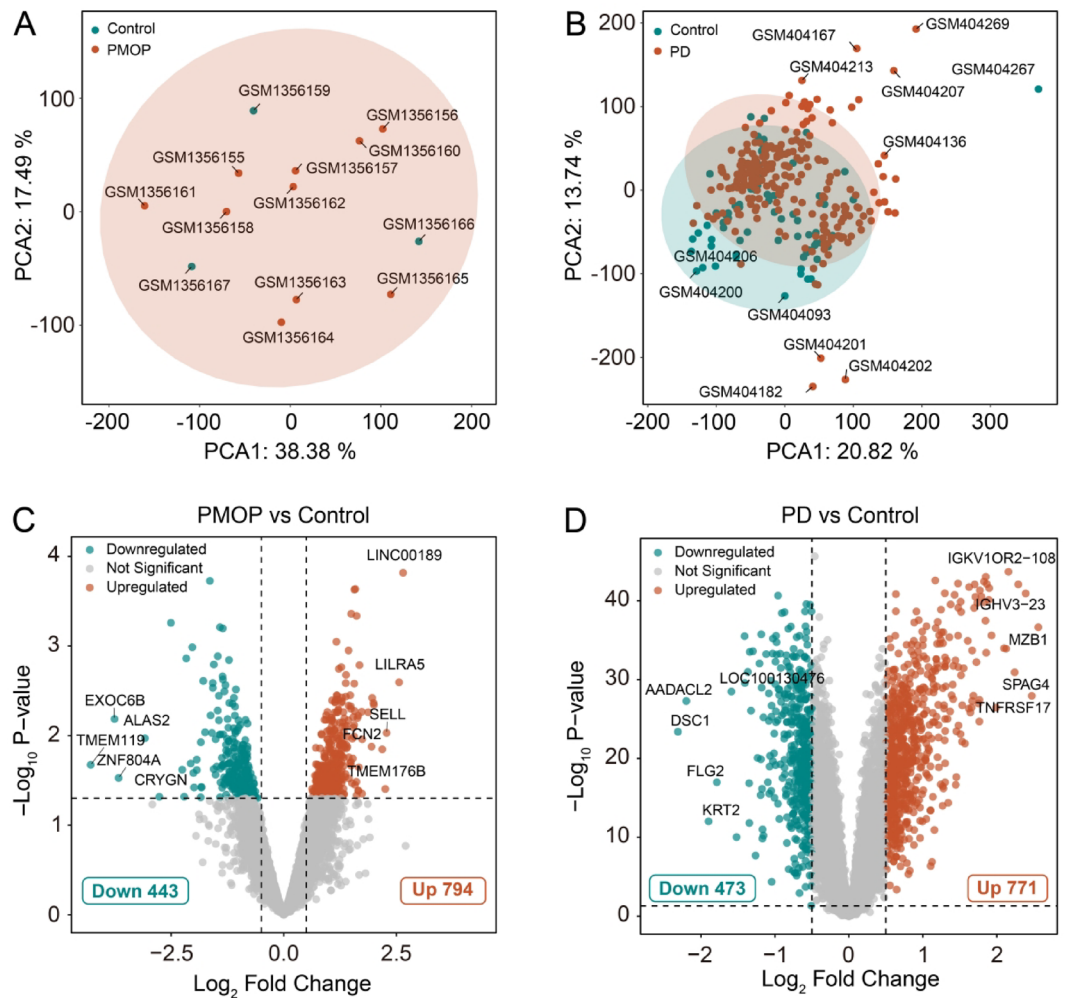


**Fig. 2.** PCA and differential expression analysis of PD and PMOP datasets **(A)** Principal component analysis (PCA) of PMOP (n = 10, orange) vs. control (n = 3, green) transcriptomes. Partial group overlap shown by 95% confidence ellipses (PC1: 38.38%, PC2: 17.49%). **(B)** PD (n = 241, orange) and control (n = 69, green) transcriptomes. Partial group overlap shown by 95% confidence ellipses (PC1: 20.82%, PC2: 13.74%). **(C)** Volcano plot of PMOP vs. control groups identifies 794 upregulated (orange) and 443 downregulated (green) genes ( $|\log_2FC| > 1.5$ ,  $FDR < 0.05$ ). Gray dots denote non-significant transcripts. Thresholds marked by dashed lines (vertical: fold change; horizontal:  $-\log_{10}[p \text{ value}]$ ). **(D)** PD vs. control analysis reveals 771 upregulated (orange) and 473 downregulated (green) DEGs under identical thresholds. Top 5 ranked DEGs by fold change are labeled (black text).

genes (Fig. 2C). Similarly, 1244 DEGs were identified for PD vs. Control, comprising 771 upregulated and 473 downregulated genes (Fig. 2D). These findings provide a robust foundation for further analysis.

### Functional analysis and the identification of candidate genes

To explore the shared mechanisms of PMOP and PD, a cross-analysis of DEGs from PMOP vs. Control and PD vs. Control was conducted, identifying 63 common DEGs (Fig. 3A). KEGG pathway analysis revealed that these genes were primarily enriched in immune and inflammatory responses (Toll-like receptor signaling pathway), cellular communication (cell adhesion molecules), and specific pathways such as osteoclast differentiation (Fig. 3B). A more detailed visualization of KEGG pathways highlighted a broad spectrum of disease-associated pathways, suggesting the involvement of these genes in the shared pathophysiological processes of PMOP and PD. Using these genes, a PPI network was constructed, identifying key hub genes such as CCR1, LILRB2, CTSS, CD14, and CCR2, which demonstrated strong interconnectivity within the network. These genes are implicated in immune responses and inflammatory signaling, underscoring their central roles in the common pathological mechanisms of PMOP and PD. Additionally, genes like MERTK and FOS, associated with Rho, were identified as potential regulators of osteoclast activity and inflammatory processes (Fig. 3C). Further analysis of DEGs co-upregulated or co-downregulated in PMOP vs. Control and PD vs. Control yielded 40 genes, which were intersected with Rho-signal transduction genes, resulting in 12 overlapping genes (Fig. 3D). These 12 genes will undergo further screening for potential biomarkers.

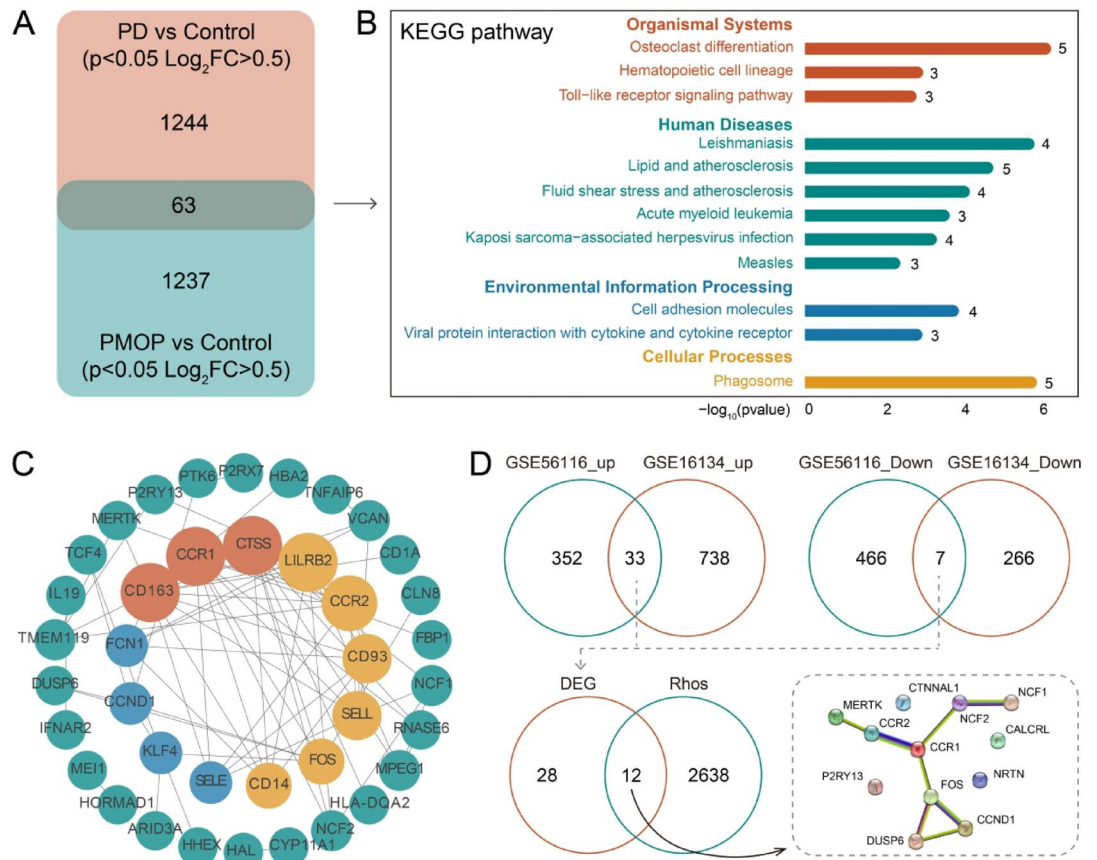


**Fig. 3.** Identification and enrichment analysis of candidate genes. **(A)** Differential expression analysis of PMOP vs Control and PD vs Control groups, yielding 1244 and 1237 DEGs, respectively, with 63 overlapping DEGs. **(B)** KEGG pathway enrichment analysis of overlapping DEGs. **(C)** Protein-protein interaction network of overlapping DEGs constructed using STRING database. **(D)** Venn diagrams showing the overlap of upregulated and downregulated DEGs between PMOP and PD datasets, and between DEGs and Rho-related genes, identifying 12 candidate genes.

### Identification of biomarkers through machine learning

To further identify potential biomarkers, Lasso regression analysis was performed on the 12 candidate genes, with three-fold cross-validation used to determine the optimal  $\log(\text{Lambda})$  value ( $\text{Lambda.min}$ ) (Fig. 4A). The corresponding genes and their coefficients, as well as the proportion of variance explained by the model, were identified (Fig. 4B). The minimum binomial deviance was 0.011 at  $\text{Lambda.min}$ , indicating the best model performance. At this point, eight genes were selected through Lasso regression: CALCRL, CCND1, CCR1, CTNNAL1, FOS, MERTK, NCF1, and NRTN. In parallel, SVM-RFE analysis was conducted to rank gene importance and identify the optimal subset based on the lowest classification error rate. The minimum error rate (0.05) was achieved when 12 genes were included in the model: FOS, NRTN, MERTK, NCF1, CCND1, P2RY13, DUSP6, CALCRL, CTNNAL1, NCF2, CTNNAL1, and CCR1 (Fig. S1A). The intersection of genes obtained from Lasso and SVM-RFE was visualized using Venn diagrams (Fig. S1B), revealing eight overlapping genes: CALCRL, CCND1, CCR1, CTNNAL1, FOS, MERTK, NCF1, and NRTN. Next, the eight candidate genes were analyzed for differential expression using the Wilcoxon test in both the PMOP dataset (Fig. 4C) and the PD dataset (Fig. 4D). Most genes showed significant differences ( $p < 0.05$ ) in both datasets. These results were further evaluated in the corresponding validation datasets. In the PD evaluation dataset (Fig. 4E), all eight genes remained significantly differentially expressed. However, in the PMOP evaluation dataset (Fig. 4F), only CTNNAL1 and MERTK maintained consistent and significant expression differences ( $p < 0.05$ ) between disease and control groups. Therefore, CTNNAL1 and MERTK were identified as the most robust and reproducible biomarkers in this study.

### Pathway enrichment and interaction network analysis of biomarkers

GSEA was conducted to assess the functional relevance of the selected biomarkers CTNNAL1 and MERTK. In PMOP and PD dataset, CTNNAL1 and MERTK were enriched in hallmark pathways related to immune response, inflammatory processes, and cell signaling (Fig. 5A–D). Additionally, a GGI network was constructed using GeneMANIA to explore interactions between these biomarkers and related genes (Fig. 5E). This network analysis revealed significant interactions of CTNNAL1 and MERTK with genes involved in functions such

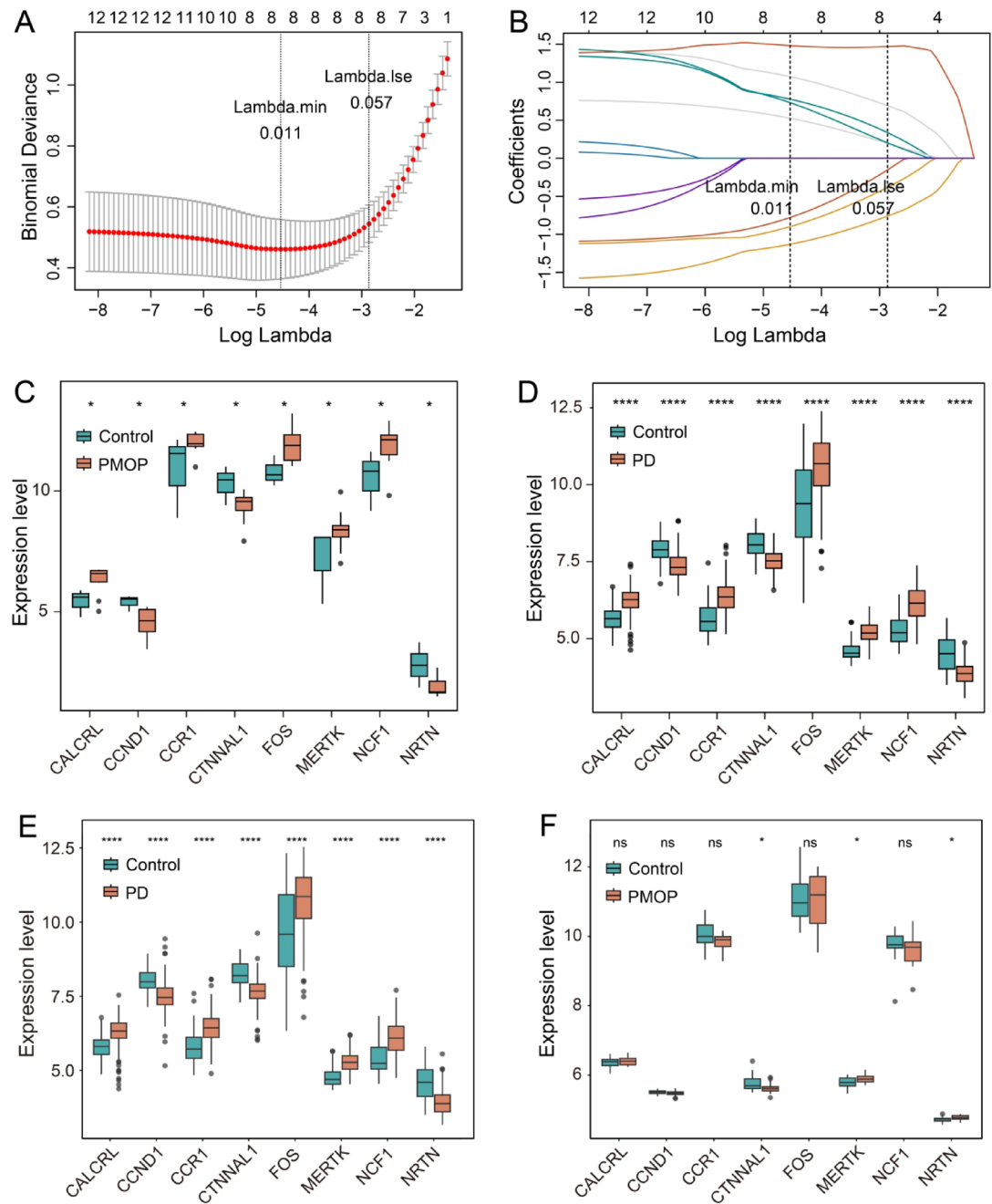


**Fig. 4.** Machine learning analysis and expression of candidate biomarkers. **(A, B)** Lasso regression analysis of 12 candidate genes with threefold cross-validation was performed to select optimal biomarkers, with Lambda.min and Lambda.1se values identified for feature selection. **(C, D)** Box plots showing expression levels of selected biomarkers in PMOP vs Control and PD vs Control groups, with significant differences indicated (\*  $p < 0.05$ , \*\*  $p < 0.01$ , \*\*\*  $p < 0.001$ , \*\*\*\*  $p < 0.0001$ ). **(E, F)** Box plots showing expression levels of selected biomarkers in PMOP evaluation dataset and PD evaluation dataset (\*  $p < 0.05$ , \*\*  $p < 0.01$ , \*\*\*  $p < 0.001$ , \*\*\*\*  $p < 0.0001$ ).

as cell–cell junctions, phagocytosis, and receptor kinase activity. A correlation analysis between CTNNAL1 and MERTK (Fig. 5F) indicated a statistically significant negative correlation (Pearson's  $r = -0.51$ ,  $p < 0.05$ ), suggesting a possible antagonistic relationship between these two biomarkers, which may have implications for their roles in disease pathways.

#### Immune infiltration analysis of CTNNAL1 and MERTK in PMOP and PD

Based on the functional analysis, we found that CTNNAL1 and MERTK are both closely associated with immune processes. To further investigate the immune landscape in PMOP and PD samples, ssGSEA was conducted to

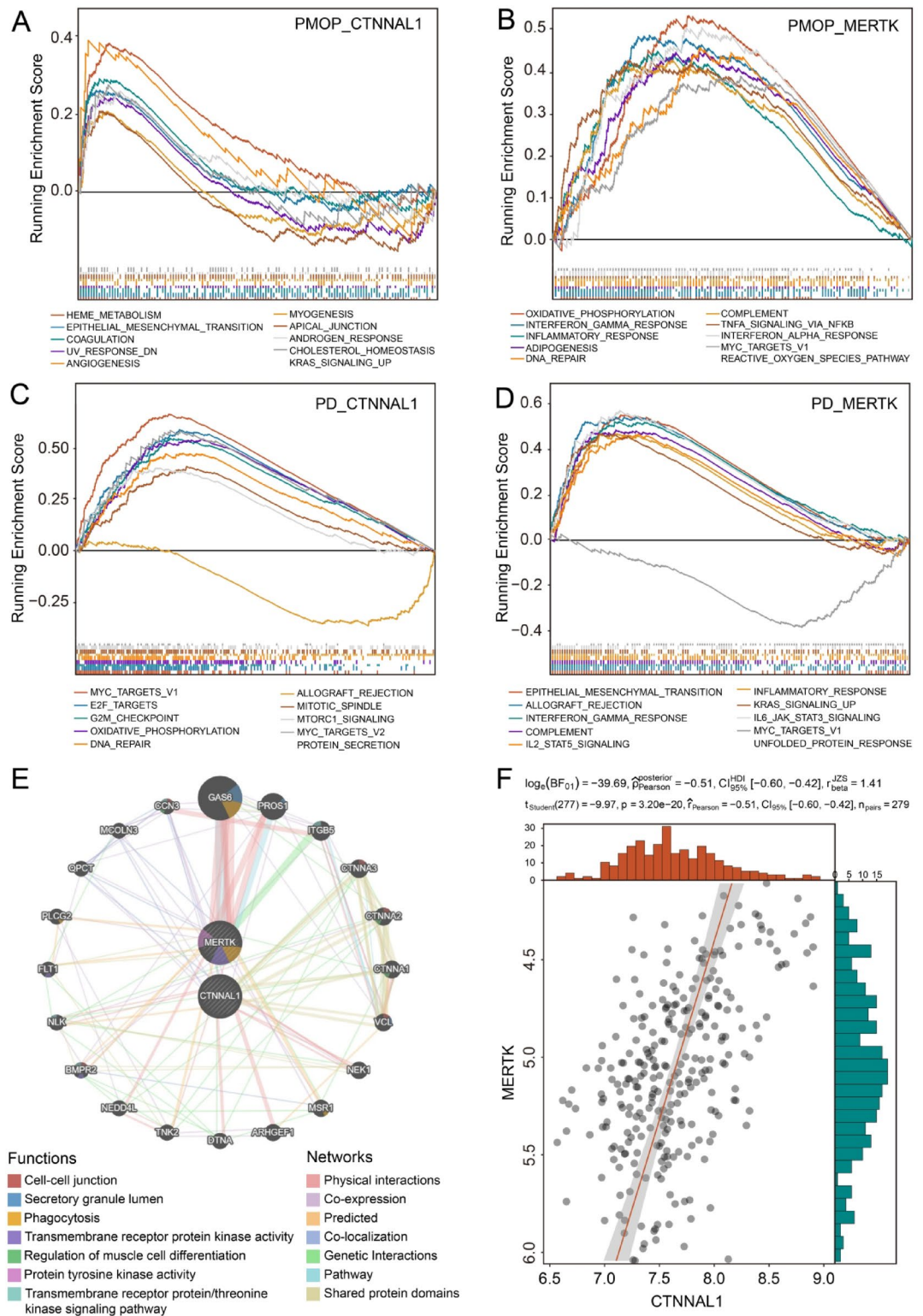


**Fig. 5.** Functional enrichment and interaction analysis of biomarkers CTNNAL1 and MERTK. (A–D) GSEA enrichment plots for CTNNAL1 and MERTK in PMOP and PD datasets. (E) Gene–Gene Interaction network constructed using GeneMANIA, illustrating interactions of CTNNAL1 and MERTK with other genes, categorized by function and interaction type. (F) Correlation analysis between CTNNAL1 and MERTK expression levels in PD dataset ( $p < 0.05$ ).

quantify immune cell infiltration across 28 immune cell types. Stacked bar plots (Fig. 6A, B) illustrate the ssGSEA scores, revealing distinct differences in immune cell proportions between the control and disease groups in both PMOP and PD samples. Box plots (Fig. 6C, D) further emphasize specific immune cell types, showing increased levels of CD56bright natural killer cells and immature dendritic cells in PMOP and PD groups compared to controls. These findings suggest that PMOP and PD are associated with an altered immune microenvironment, potentially mediated by the identified biomarkers.

To explore the relationship between CTNNAL1 and MERTK and these immune cells, we performed Spearman correlation analysis between the biomarkers and differentially infiltrated immune cells. The results revealed that CTNNAL1 expression was negatively correlated with the abundance of differentially infiltrated immune cells in PMOP and PD samples, indicating a potential association with immune infiltration status. In contrast, MERTK showed positive correlations with these immune cells, indicating that MERTK expression was positively associated with immune infiltration (Fig. 6E).

### Regulatory networks of CTNNAL1 and MERTK

To further explore the potential regulatory mechanisms involving CTNNAL1 and MERTK, we constructed lncRNA-miRNA-mRNA and circRNA-miRNA-mRNA interaction networks. The lncRNA-miRNA-mRNA network (Fig. 7A) highlights key regulators such as XIST, GAS5, and NEAT1, which may function as competing endogenous RNAs, sponging miRNAs to modulate the expression of CTNNAL1 and MERTK. Similarly, the circRNA-miRNA-mRNA network identifies interactions where circRNAs, such as hsa\_circ\_003824, may act as stable molecular sponges to regulate miRNAs targeting these biomarkers. Additionally, MERTK appears to be regulated by several TFs, including KLF6, FOSL1, and GATA1, which are involved in immune responses and inflammation. In contrast, CTNNAL1 is associated with TFs such as HDAC1, JUNB, and ATF1, suggesting its involvement in transcriptional regulation and cellular stress responses (Fig. 7B). These regulatory networks may influence pathways related to osteoclast differentiation and immune cell infiltration, playing a role in maintaining tissue homeostasis or contributing to bone loss and inflammation in PMOP and PD. These findings provide insights into the molecular mechanisms underlying the diseases and highlight potential targets for therapeutic intervention.

### Subcellular localization, chromosomal mapping, and disease association of biomarkers

At last, subcellular localization analysis was performed to predict the cellular compartments where CTNNAL1 and MERTK predominantly reside. Both biomarkers were found to localize mainly to the nucleus and cytoplasm, with lower proportions in the extracellular region and endoplasmic reticulum (Fig. 8A). Chromosomal mapping placed CTNNAL1 on chromosome 9 and MERTK on chromosome 2 (Fig. 8B), providing a genomic context for these biomarkers. Disease association analysis, based on InferenceScores from the CTD database, indicated strong associations of both biomarkers with a range of immune system and metabolic diseases (Fig. 8C, D). CTNNAL1 and MERTK were notably linked to conditions such as immune system disorders, metabolic syndrome, insulin resistance, and dyslipidemias, highlighting their potential roles in systemic disease processes beyond PD and PMOP. This analysis suggests that CTNNAL1 and MERTK may act as intersectional biomarkers, connecting local inflammatory responses in PD and PMOP to broader metabolic and immune regulatory mechanisms.

### Experimental validation in OP+PD animal model

To experimentally validate the findings from bioinformatics analyses, we established an OP+PD mouse model (Fig. S2A–C). Histological staining revealed reduced trabecular bone in femoral and periodontal tissues in the OP+PD group compared with Sham controls (Fig. 9A). Methylene blue staining showed increased alveolar bone resorption in OP+PD mice. Serum inflammatory cytokines including TNF- $\alpha$ , IL-1 $\beta$ , IL-6, and IL-4 were significantly elevated in OP+PD mice (Fig. 9B). RT-qPCR results indicated that CTNNAL1 was significantly downregulated while MERTK was upregulated in gingival tissues of OP+PD mice (Fig. 9C). Consistently, Western blot analysis confirmed decreased CTNNAL1 protein levels and increased MERTK expression in the OP+PD group compared to Sham (Fig. 9D; Fig. S3). These *in vivo* results support the potential regulatory roles of CTNNAL1 and MERTK in bone loss and inflammation in PMOP and PD.

### Discussion

PMOP and PD are prevalent chronic conditions characterized by bone loss. Emerging evidence suggests that Rho play a pivotal role in the pathogenesis of both diseases by regulating osteoblast and osteoclast activities, thereby influencing bone remodeling processes. Understanding the involvement of Rho in PMOP and PD is a new direction for developing risk predictors and targeted therapeutic strategies.

In this study, we identified DEGs associated with PD and PMOP. KEGG enrichment analyses revealed significant pathways, including leishmaniasis and osteoclast differentiation. The leishmaniasis pathway has been implicated in bone resorption processes, which are relevant to both PD and PMOP<sup>24</sup>. The osteoclast differentiation pathway is directly involved in bone remodeling and has been linked to the pathogenesis of osteoporosis and PD<sup>9</sup>. It should be noted that the PMOP and PD datasets used in this study were derived from peripheral blood and gingival tissue, respectively, which differ in tissue type and cellular composition. Although both diseases are closely associated with immune dysregulation, such heterogeneity in tissue sources may affect the interpretation of shared DEGs and biomarkers. Therefore, our findings should be viewed as exploratory, and further validation in datasets derived from comparable tissue sources is warranted to confirm the biological relevance and applicability of these markers.

Then intersected DEGs with Rho-signal transduction genes, resulting in 12 candidate genes. Utilizing machine learning algorithms, we identified CTNNAL1 and MERTK as potential biomarkers. CTNNAL1 has been associated with bone metabolism and osteoclast activity, suggesting its role in bone resorption processes<sup>24</sup>.

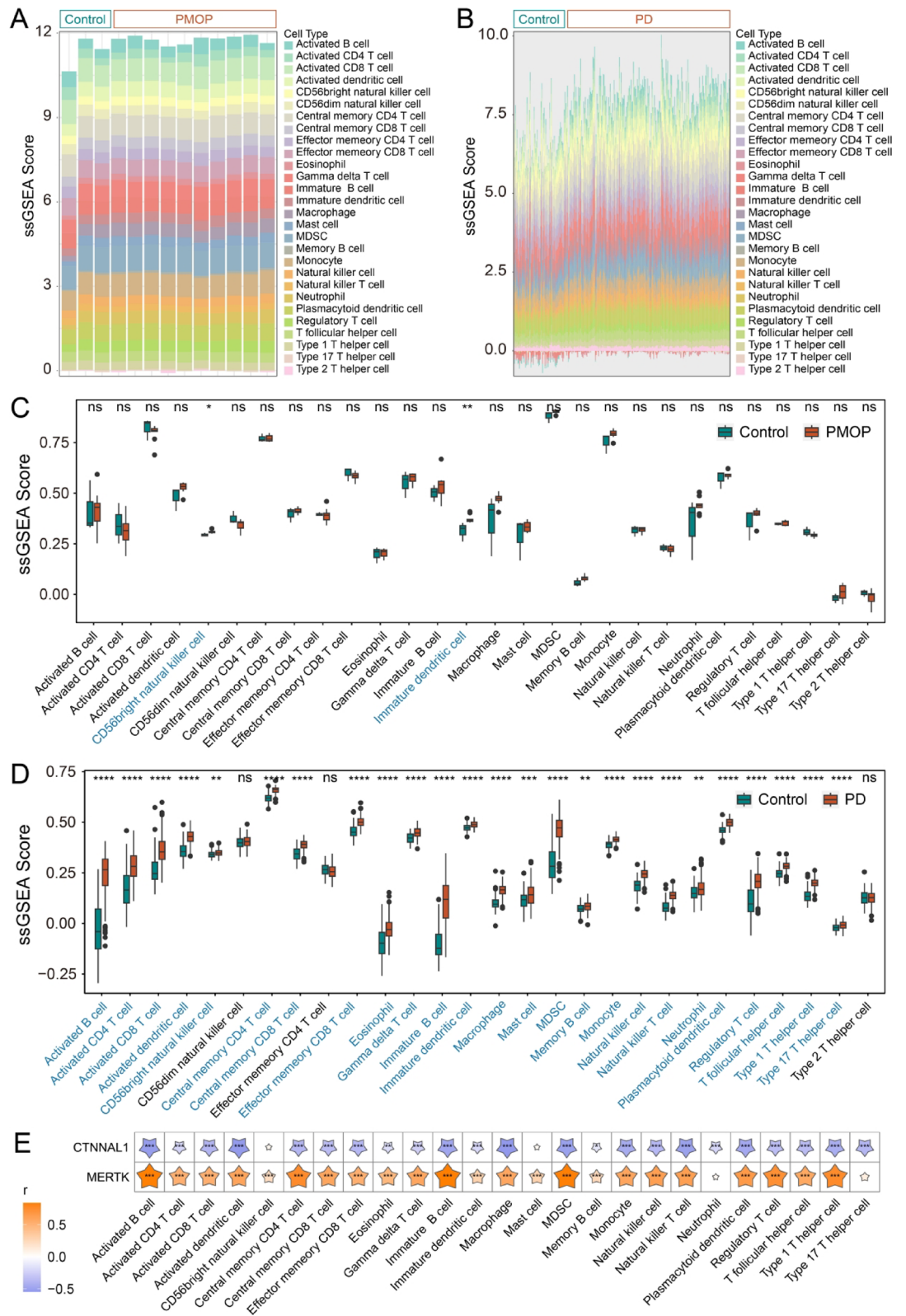


**Fig. 6.** Immune infiltration analysis of PD and PMOP samples. **(A, B)** Stacked bar plots showing single-sample Gene Set Enrichment Analysis (ssGSEA) scores for 28 immune cell types in Control and PMOP, and Control and PD groups. **(C, D)** Box plots of ssGSEA scores comparing immune cell infiltration between Control and PMOP, and Control and PD groups, with specific cell types highlighted in red where significant changes were observed. **(E)** Spearman correlation analysis using PD dataset between biomarkers and differential immune cells (\*  $p < 0.05$ , \*\*  $p < 0.01$ , \*\*\*  $p < 0.001$ , \*\*\*\*  $p < 0.0001$ ).

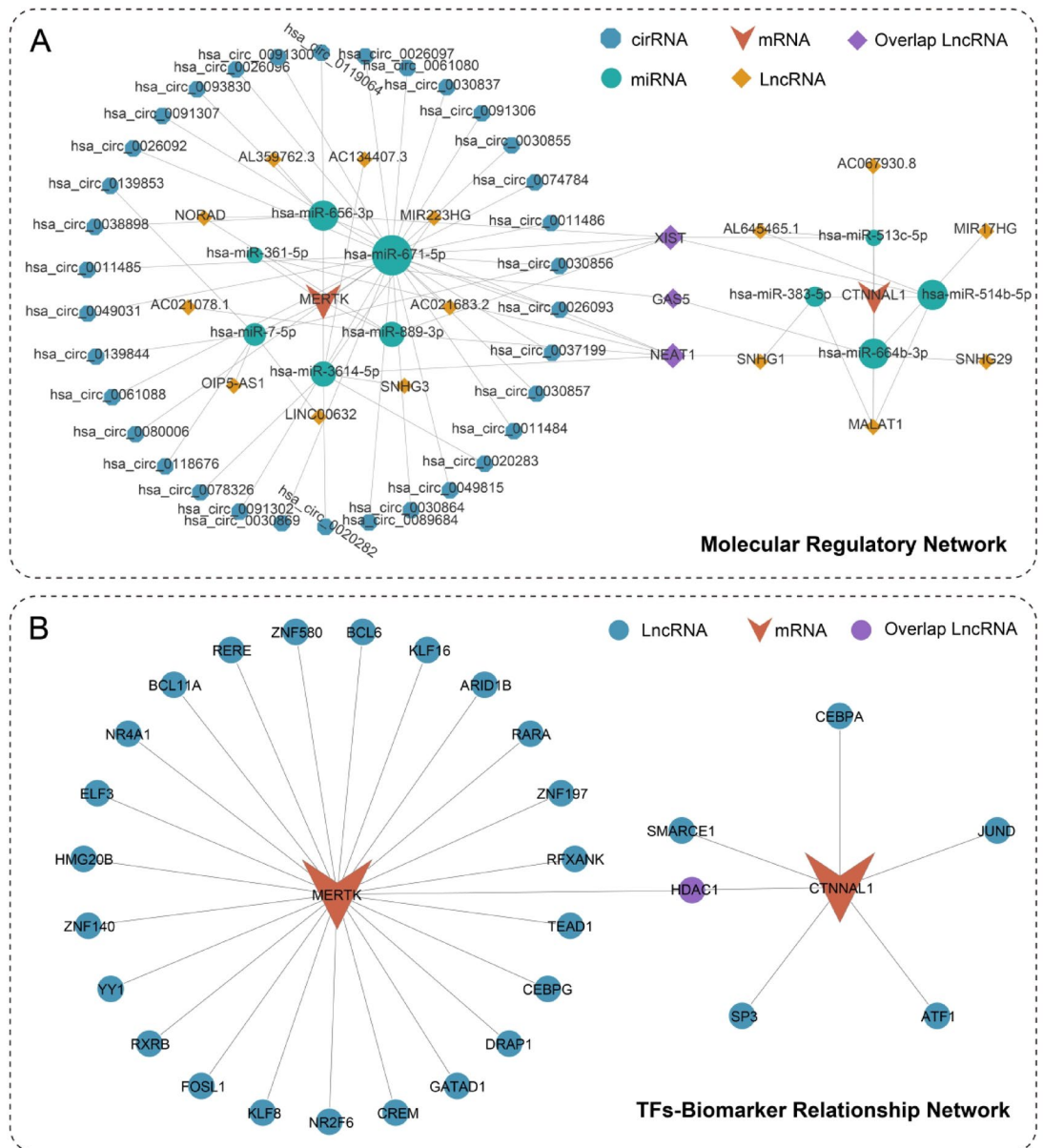


**Fig. 7.** Molecular regulatory networks for biomarkers CTNNAL1 and MERTK. **(A)** Predicted circRNA–miRNA–mRNA and lncRNA–miRNA–mRNA interaction networks for CTNNAL1 and MERTK, showing regulatory connections with non-coding RNAs (circRNAs, lncRNAs) targeting miRNAs that interact with CTNNAL1 and MERTK. **(B)** Transcription factors (TFs) network for CTNNAL1 and MERTK, displaying TFs predicted to regulate these biomarkers. Arrows indicate regulatory interactions, with key TFs highlighted.

MERTK is involved in immune regulation and has been linked to inflammatory responses in bone tissues, indicating its potential involvement in the inflammatory aspects of PMOP and PD<sup>9</sup>. Our study is among the first to highlight the association of CTNNAL1 and MERTK with both PMOP and PD, providing new insights into their roles in these diseases.

To investigate the functions of CTNNAL1 and MERTK, a GSEA was performed, revealing enrichment in pathways such as allograft rejection and oxidative phosphorylation. The allograft rejection pathway involves immune responses that may contribute to the inflammatory environment characteristic of PMOP and PD. Oxidative phosphorylation, essential for cellular energy metabolism, has been implicated in bone loss and periodontal disease when dysregulated. In recent years, studies have highlighted the critical role of inflammation and immune responses in PMOP and PD<sup>25</sup>. These processes, mediated by the activation of immune cells and pro-inflammatory cytokines such as TNF- $\alpha$ , IL-1, and IL-6, significantly impact bone homeostasis. Inflammation activates the NF- $\kappa$ B signaling pathway, promoting osteoclastogenesis while suppressing osteoblast differentiation and activity, leading to an imbalance in bone remodeling and eventual bone loss<sup>26</sup>. Additionally, the interaction between the complement system and NF- $\kappa$ B signaling further exacerbates inflammatory responses, driving both localized bone loss (e.g., alveolar bone) and systemic bone loss (e.g., osteoporosis). This interplay represents a

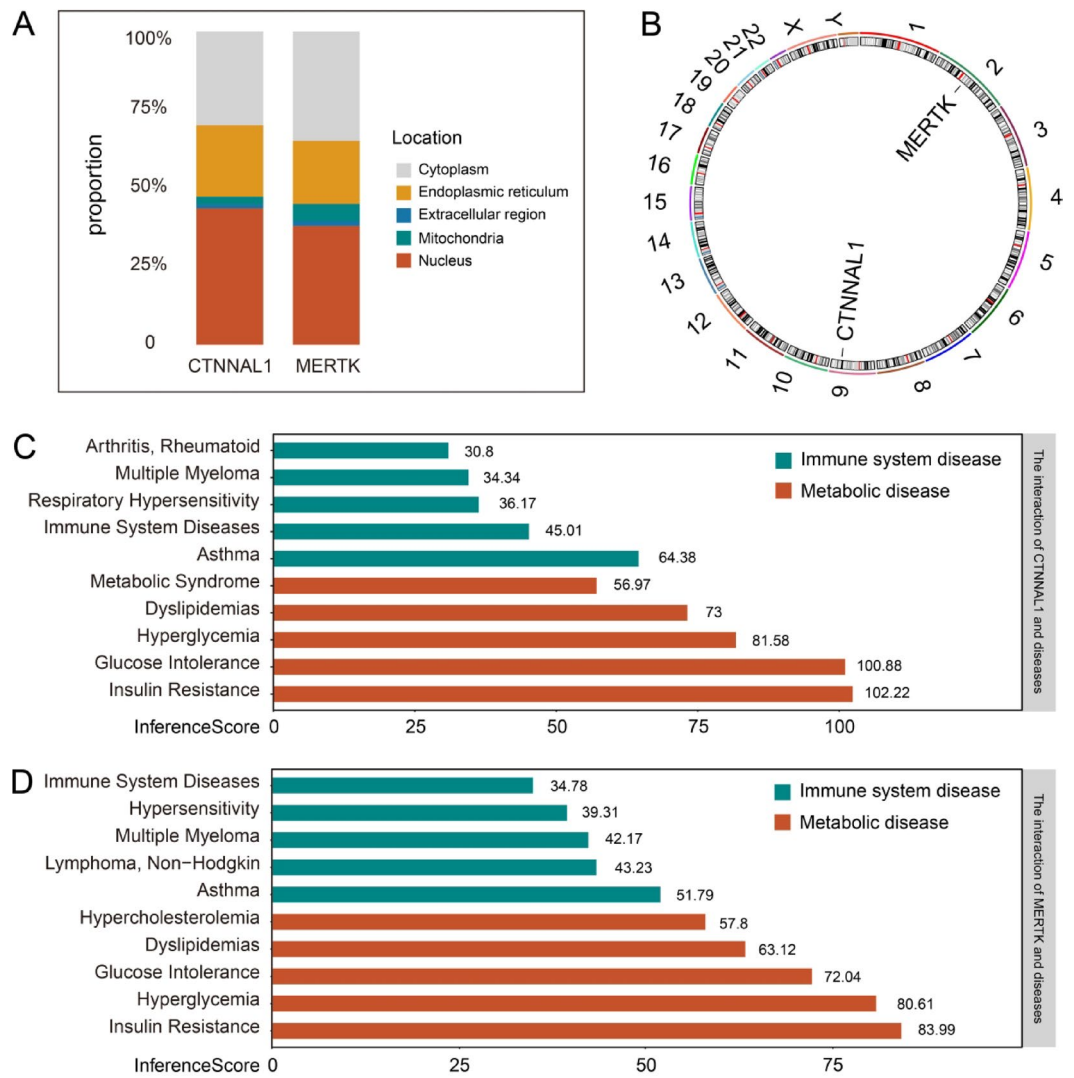


**Fig. 8.** Subcellular localization, chromosomal mapping, and disease association analysis of biomarkers CTNNAL1 and MERTK. **(A)** Predicted subcellular localization of CTNNAL1 and MERTK across different cellular compartments. **(B)** Chromosomal locations of CTNNAL1 (chromosome 9) and MERTK (chromosome 2), displayed on a circular chromosome map. **(C, D)** Disease association analysis for CTNNAL1 and MERTK with immune and metabolic diseases, ranked by InferenceScore.

key mechanistic link between PMOP and PD<sup>5</sup>. Clinical studies have also investigated the immune environment in PMOP and PD. For instance, one study analyzing the relationship between plasma 25-hydroxyvitamin D levels and salivary/serum C-reactive protein concentrations in 567 postmenopausal women found an inverse correlation between vitamin D status and salivary CRP, but no significant association with serum CRP<sup>27</sup>. Taken together, these findings underscore the importance of identifying biomarkers and elucidating key mechanisms to facilitate clinical translation and the development of targeted therapeutic strategies.

Immune infiltration analysis was subsequently performed, showing pronounced differences in the levels of CD56bright natural killer cells and immature dendritic cells between the disease and control groups. These immune cells are critical in modulating inflammatory responses and bone remodeling. Elevated levels of these cells have been linked to increased osteoclast activity and bone resorption, thereby contributing to the pathogenesis of PMOP and PD. Interestingly, CTNNAL1 showed negative correlations with these differentially infiltrated immune cells, suggesting that it may play a role in immune cell infiltration in PMOP and PD. Conversely, MERTK demonstrated positive correlations with these immune cells, indicating its potential role in immune cell infiltration and contributing to the inflammatory environment associated with these conditions.

Next, we constructed regulatory networks incorporating lncRNAs, miRNAs, and TFs associated with CTNNAL1 and MERTK. Among these, lncRNA XIST and HDAC1 were identified as potential key regulators. XIST has been implicated in osteogenic differentiation and bone metabolism, highlighting its potential role in bone-related diseases. HDAC1, known for its involvement in chromatin remodeling and gene expression

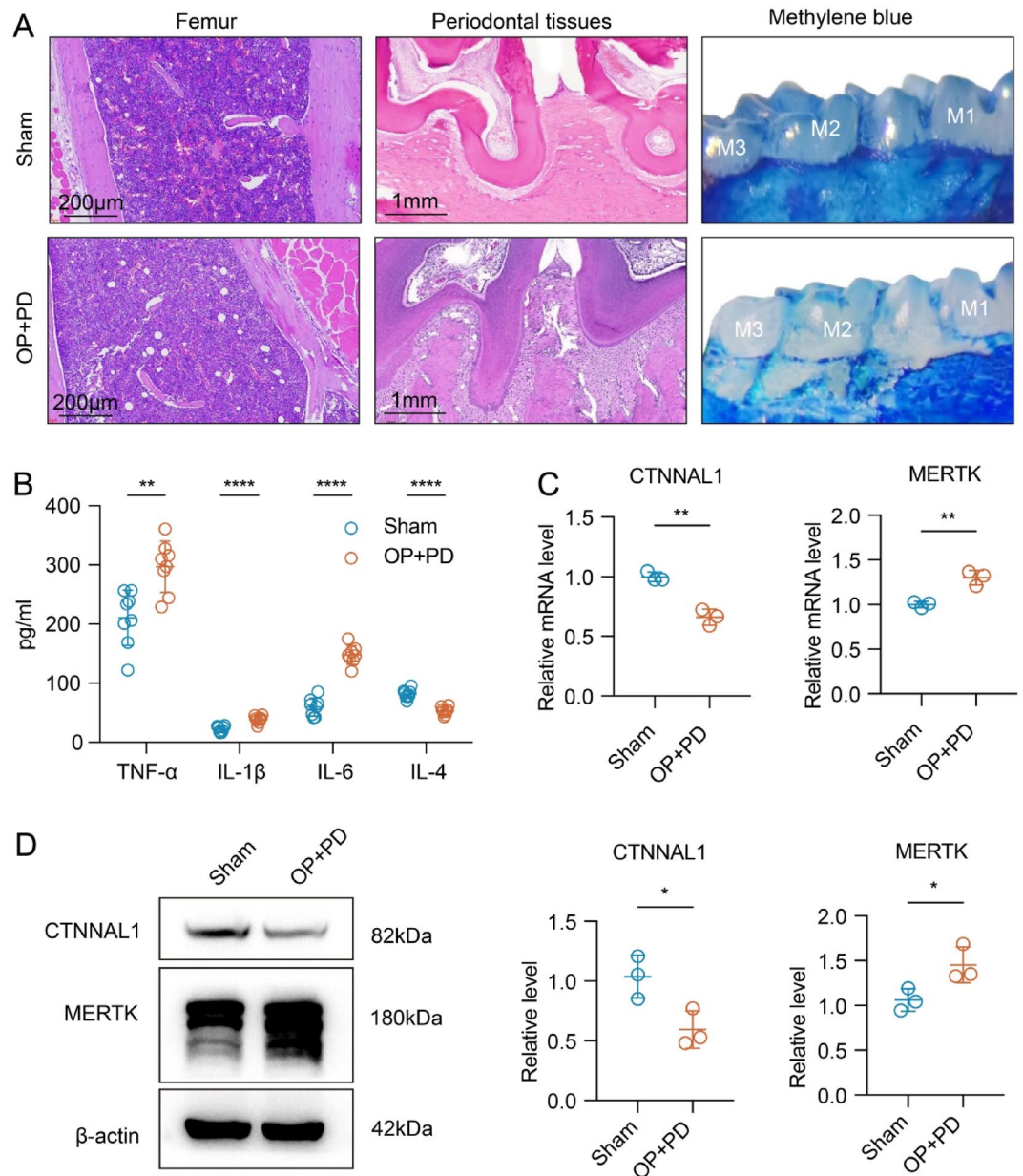


**Fig. 9.** In vivo validation of CTNNAL1 and MERTK expression in the OP+PD mouse model. (A) H&E staining of femur and periodontal tissues, and methylene blue staining of alveolar bone in Sham and OP+PD groups. Scale bars as indicated. (B) ELISA results of serum inflammatory cytokines (TNF- $\alpha$ , IL-1 $\beta$ , IL-6, IL-4) between Sham and OP+PD groups. (C) Relative mRNA levels of CTNNAL1 and MERTK in gingival tissues measured by RT-qPCR. (D) Western blot and corresponding quantification of CTNNAL1 and MERTK expression in gingival tissues.  $\beta$ -actin was used as internal control. Data are shown as mean  $\pm$  SD. \* $p$  < 0.05, \*\* $p$  < 0.01, \*\*\*\* $p$  < 0.0001.

regulation, influences both osteoclast activity and inflammatory responses. These regulatory elements may modulate the expression of CTNNAL1 and MERTK, thereby impacting disease progression.

Furthermore, subcellular localization analysis revealed that CTNNAL1 and MERTK are predominantly localized in the nucleus and cytoplasm, suggesting their roles in transcriptional regulation and intracellular signaling pathways. Disease association analysis uncovered links to conditions such as insulin resistance, which has been associated with both PMOP and PD. This indicates that CTNNAL1 and MERTK may act as intersectional biomarkers, bridging localized inflammatory responses in PMOP and PD with broader metabolic and immune regulatory mechanisms.

This study utilized bioinformatics approaches to explore the role of Rho-signal transduction genes in PMOP and periodontitis PD, identifying CTNNAL1 and MERTK as key biomarkers. Our findings provide insights into the molecular interplay between these two diseases and highlight potential therapeutic targets. Despite the identification of biomarkers, several limitations should be acknowledged that may impact the interpretation

and clinical relevance of our findings. One limitation lies in the DEG selection criteria. We adopted a relatively lenient threshold ( $|\log_2FC| > 0.5$ ,  $p < 0.05$ ) to enhance sensitivity to moderate expression changes. However, we acknowledge that using unadjusted  $p$  values and a lower fold-change cutoff increases the likelihood of false positives. To improve reliability, we incorporated multiple validation layers, including consistency analysis across independent datasets, machine learning-based feature selection, and in vivo experimental confirmation. Furthermore, the clinical applicability of our findings is constrained by the relatively small sample sizes and the lack of external cohort validation. Future studies should address these limitations by including larger, more diverse populations and conducting additional functional and clinical validation. Translating these findings into practical diagnostic or therapeutic tools will also require careful consideration of feasibility, cost-effectiveness, and clinical utility.

### Data availability

All data analyzed in this study are available in the Gene Expression Omnibus (GEO) database (details in the method). Additional materials are available upon request from the corresponding author.

Received: 2 December 2024; Accepted: 28 July 2025

Published online: 05 August 2025

### References

- Arceo-Mendoza, R. M. & Camacho, P. M. Postmenopausal osteoporosis: Latest guidelines. *Endocrinol. Metab. Clin. North Am.* **50**(2), 167–178 (2021).
- Papapanou, P. N. et al. Periodontitis: Consensus report of workgroup 2 of the 2017 world workshop on the classification of periodontal and peri-implant diseases and conditions. *J. Periodontol.* **89**(Suppl 1), S173–S182 (2018).
- Passos, J. S. et al. Osteoporosis/osteopenia as an independent factor associated with periodontitis in postmenopausal women: A case-control study. *Osteoporos. Int.* **24**(4), 1275–1283 (2013).
- Qi, J. et al. Association between periodontal disease and osteoporosis in postmenopausal women: A systematic review and meta-analysis. *Heliyon* **9**(11), e20922 (2023).
- Yu, B. & Wang, C. Y. Osteoporosis and periodontal diseases—An update on their association and mechanistic links. *Periodontol.* **2000** **89**(1), 99–113 (2022).
- Dong, Q. et al. RhoA/ROCK1 regulates the mitochondrial dysfunction through Drp1 induced by *Porphyromonas gingivalis* in endothelial cells. *J. Cell. Mol. Med.* **27**(15), 2123–2135 (2023).
- Mosaddeghzadeh, N. & Ahmadian, M. R. The RHO family GTPases: Mechanisms of regulation and signaling. *Cells* **10**(7), 1831 (2021).
- Jaffe, A. B. & Hall, A. Rho GTPases: Biochemistry and biology. *Annu. Rev. Cell Dev. Biol.* **21**, 247–269 (2005).
- Wang, J. et al. RhoA promotes osteoclastogenesis and regulates bone remodeling through mTOR-NFATc1 signaling. *Mol. Med.* **29**(1), 49 (2023).
- Teitelbaum, S. L. Osteoclasts: What do they do and how do they do it?. *Am. J. Pathol.* **170**(2), 427–435 (2007).
- Yamamoto, T. et al. Modulation of microenvironment for controlling the fate of periodontal ligament cells: The role of Rho/ROCK signaling and cytoskeletal dynamics. *J. Cell. Commun. Signal* **12**(1), 369–378 (2018).
- Xie, L. et al. Comparisons of gene expression between peripheral blood mononuclear cells and bone tissue in osteoporosis. *Medicine* **102**(20), e33829 (2023).
- Krebschull, M. et al. Gingival tissue transcriptomes identify distinct periodontitis phenotypes. *J. Dent. Res.* **93**(5), 459–468 (2014).
- Zhou, Y. et al. A novel approach for correction of crosstalk effects in pathway analysis and its application in osteoporosis research. *Sci. Rep.* **8**(1), 668 (2018).
- Demmer, R. T. et al. Transcriptomes in healthy and diseased gingival tissues. *J. Periodontol.* **79**(11), 2112–2124 (2008).
- Ritchie, M. E. et al. Limma powers differential expression analyses for RNA-sequencing and microarray studies. *Nucleic Acids Res.* **43**(7), e47 (2015).
- Cao, T., Li, Q., Huang, Y. & Li, A. PlotnineSeqSuite: A python package for visualizing sequence data using ggplot2 style. *BMC Genomics* **24**(1), 585 (2023).
- Kanehisa, M., Furumichi, M., Sato, Y., Ishiguro-Watanabe, M. & Tanabe, M. KEGG: Integrating viruses and cellular organisms. *Nucleic Acids Res.* **49**(D1), D545–D551 (2021).
- Yu, G., Wang, L. G., Han, Y. & He, Q. Y. ClusterProfiler: An R package for comparing biological themes among gene clusters. *OMICS* **16**(5), 284–287 (2012).
- Liu, Y. et al. A multi-omics analysis of NASH-related prognostic biomarkers associated with drug sensitivity and immune infiltration in hepatocellular carcinoma. *J. Clin. Med.* **12**(4), 1286 (2023).
- Robles-Jimenez, L. E. et al. Worldwide traceability of antibiotic residues from livestock in wastewater and soil: A systematic review. *Animals* **12**(1), 60 (2021).
- Slater, N. et al. High-resolution HLA genotyping in inclusion body myositis refines 8.1 ancestral haplotype association to DRB1\*03:01:01 and highlights pathogenic role of arginine-74 of DRbeta1 chain. *J. Autoimmun.* **142**, 103150 (2024).
- Zhang, H., Meltzer, P. & Davis, S. RCircos: An R package for circos 2D track plots. *BMC Bioinform.* **14**, 244 (2013).
- Jayusman, P. A. et al. Overview on postmenopausal osteoporosis and periodontitis: The therapeutic potential of phytoestrogens against alveolar bone loss. *Front. Pharmacol.* **14**, 1120457 (2023).
- Xu, L. et al. Osteoblast-specific down-regulation of NLRP3 inflammasome by aptamer-functionalized liposome nanoparticles improves bone quality in postmenopausal osteoporosis rats. *Theranostics* **14**(10), 3945–3962 (2024).
- Yang, Y. J. et al. Tubson-2 decoction ameliorates rheumatoid arthritis complicated with osteoporosis in CIA rats involving isochlorogenic acid A regulating IL-17/MAPK pathway. *Phytomedicine* **116**, 154875 (2023).
- Twardowski, S. E. et al. Plasma 25-hydroxyvitamin D concentrations and serum and salivary C-reactive protein in the osteoporosis and periodontal disease study. *Nutrients* **13**(4), 1148 (2021).

### Acknowledgements

We thank The First School of Clinical Medicine, Lanzhou and Stomatology Center of Gansu Provincial Hospital for their support on our works.

### Author contributions

J Q and J W designed the study, conducted data analysis, and drafted the manuscript. E L contributed to the bioinformatics analysis and manuscript editing. Y P and Y W provided critical revision and supervision. All authors

read and approved the final manuscript.

### Funding

This study was supported by Science–Technology Foundation for the health care industry of Gansu Province of China (Grant no. GSWSKY2020-77) and Youth Incubation Research Program Gansu Provincial Hospital of China (Grant no. 23GSSYF-35).

### Declarations

#### Competing interests

The authors declare no competing interests.

#### Ethics approval and consent to participate

The study complies with the ARRIVE guidelines (<https://arriveguidelines.org>). All animal experiments were approved by the Ethics Committee of Gansu Provincial Hospital (Approval No. 2022-13) and conducted in accordance with institutional guidelines.

#### Consent for publication

All authors have agreed to the publication of this article.

#### Additional information

**Supplementary Information** The online version contains supplementary material available at <https://doi.org/10.1038/s41598-025-13872-w>.

**Correspondence** and requests for materials should be addressed to J.W.

**Reprints and permissions information** is available at [www.nature.com/reprints](http://www.nature.com/reprints).

**Publisher's note** Springer Nature remains neutral with regard to jurisdictional claims in published maps and institutional affiliations.

**Open Access** This article is licensed under a Creative Commons Attribution-NonCommercial-NoDerivatives 4.0 International License, which permits any non-commercial use, sharing, distribution and reproduction in any medium or format, as long as you give appropriate credit to the original author(s) and the source, provide a link to the Creative Commons licence, and indicate if you modified the licensed material. You do not have permission under this licence to share adapted material derived from this article or parts of it. The images or other third party material in this article are included in the article's Creative Commons licence, unless indicated otherwise in a credit line to the material. If material is not included in the article's Creative Commons licence and your intended use is not permitted by statutory regulation or exceeds the permitted use, you will need to obtain permission directly from the copyright holder. To view a copy of this licence, visit <http://creativecommons.org/licenses/by-nc-nd/4.0/>.

© The Author(s) 2025